

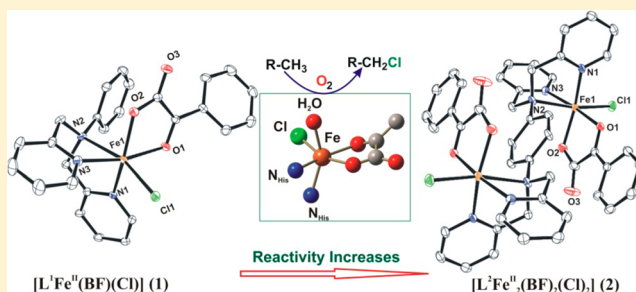
Aliphatic C–H Bond Halogenation by Iron(II)- α -Keto Acid Complexes and O₂: Functional Mimicking of Nonheme Iron Halogenases

Rahul Dev Jana, Debobrata Sheet, Sayanti Chatterjee, and Tapan Kanti Paine*

Department of Inorganic Chemistry, Indian Association for the Cultivation of Science, 2A & 2B Raja S. C. Mullick Road, Jadavpur, Kolkata 700032, India

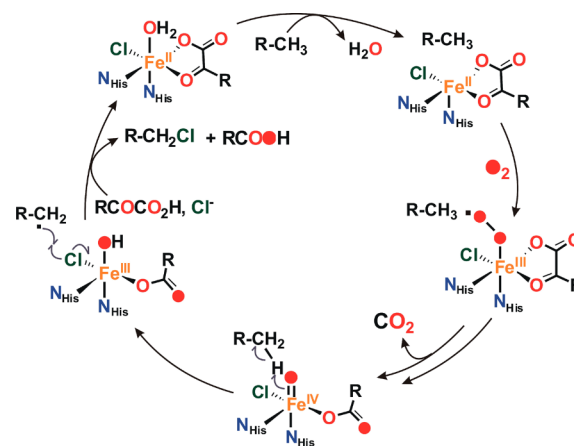
Supporting Information

ABSTRACT: α -Ketoglutarate-dependent nonheme halogenases catalyze the halogenation of aliphatic C–H bonds in the biosynthesis pathway of many natural products. An iron(IV)-oxo-halo species has been established as the active oxidant in the halogenation reactions. With an objective to emulate the function of the nonheme halogenases, two iron(II)- α -keto acid complexes, [(phdpa)Fe(BF)Cl] (1) and [(1,4-tpbd)Fe₂(BF)₂Cl₂] (2) (where phdpa = *N,N*-bis(2-pyridylmethyl)aniline, 1,4-tpbd = *N,N,N',N'*-tetrakis(2-pyridylmethyl)benzene-1,4-diamine, and BF = benzoylformate), have been prepared. The iron complexes are capable of carrying out the oxidative halogenation of aliphatic C–H bonds using O₂ as the terminal oxidant. Although the complexes are not selective toward C–H bond halogenation, they are the only examples of nonheme iron(II)- α -keto acid complexes mimicking the activity of nonheme halogenases. The dinuclear complex (2) exhibits enhanced reactivity toward C–H bond halogenation/hydroxylation.



INTRODUCTION

The halogenation of aliphatic C–H bonds is a unique chemical reaction in biology. Biosyntheses of a large variety of natural products involve the halogenation of unactivated C–H bonds at aliphatic carbon centers. In the biosynthetic processes, α -ketoglutarate (α -KG)-dependent nonheme iron halogenases activate O₂ to halogenate aliphatic C–H bonds of substrates.¹ CytC3 and SyrB2 are examples of this group of enzymes involved in the biosynthesis of cytostriatin A/B and syringomycin E.^{2,3} Crystal structures of several α -KG-dependent halogenases have been determined.^{4–6} The structure of SyrB2 reveals that the iron(II) center is coordinated by two nitrogen atoms from histidine residues, a chloride anion, one water, and a bidentate α -KG cofactor.⁴ The catalytic mechanism has been proposed to follow a pathway similar to that of α -KG-dependent oxygenases. The reductive activation of dioxygen at the iron center with concomitant decarboxylation of α -ketoglutarate results in an iron(IV)-oxo-chloro species (Scheme 1). The high-valent iron-oxo intermediate abstracts a hydrogen atom from the substrate to initiate the halogenation reaction.^{2,3,7,8} The substrate radical then combines with the chloride radical producing chlorinated product and regenerating the reduced iron(II) center. After formation of the substrate carbon radical, however, competition between transfer of Cl[•] and OH[•] would be expected. No hydroxylation reaction has been observed in enzymatic systems indicating that Cl[•] transfer is the most favored pathway. The hydrogen bonding pattern at the active site and the lower potential of Cl[•] versus OH[•] likely contribute to the

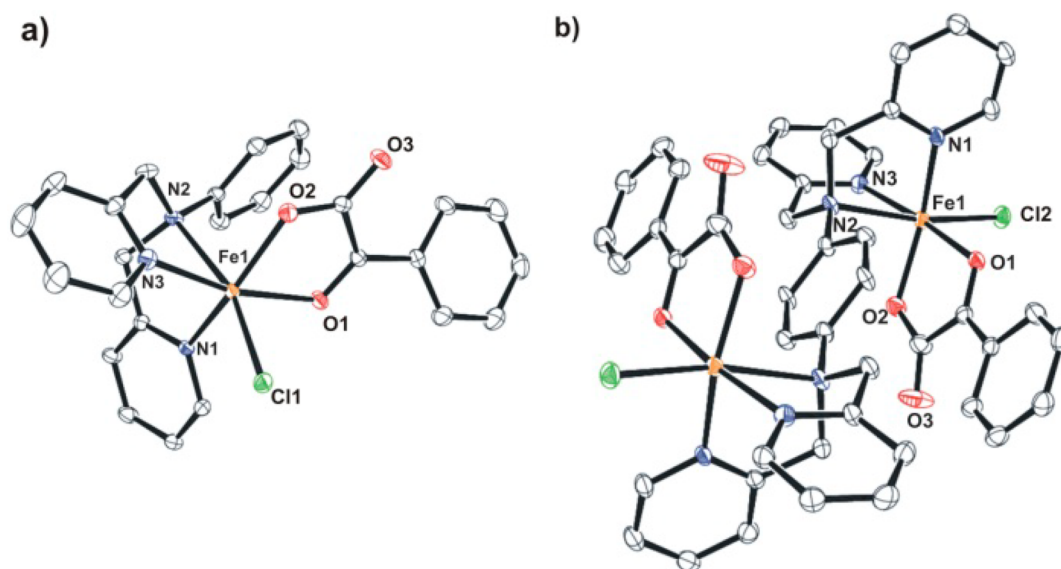
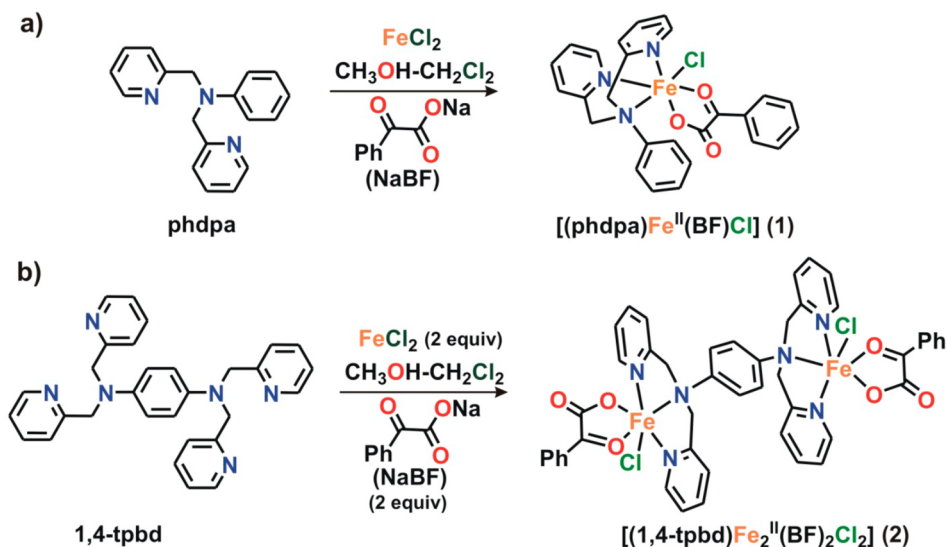
Scheme 1. Proposed Catalytic Cycle of α -Ketoglutarate-Dependent Halogenases

selectivity.^{9,10} Thorough experimental studies on SyrB2 suggested that substrate positioning was a crucial criterion for controlling the enzyme selectivity.^{9,11} Computational studies indicated that the halogenation selectivity originated from the deactivation of the hydroxyl radical rebound site either by protonation of the hydroxyl group¹² or by the CO₂ formed in the halogenation cycle.¹³

Received: February 15, 2018

Published: July 16, 2018

Scheme 2. Synthesis of Iron(II)-Benzoylformate Complexes

Figure 1. ORTEP plot of (a) $[(\text{phdpa})\text{Fe}(\text{BF})\text{Cl}]$ (1) and (b) $[(1,4\text{-tpbd})\text{Fe}_2(\text{BF})_2\text{Cl}_2]$ (2). All the hydrogen atoms have been omitted for clarity.

Though there have been extensive studies on the enzymatic structure and function of nonheme halogenases, examples of synthetic models of this group of enzymes are rare.^{14–20} Several iron(IV)-oxo-halo complexes, that mimic the active oxidant of nonheme halogenases, have been isolated and characterized.^{15,21,22} Among the reported complexes, the $S = 1$ iron(IV)-oxo-halo complexes of tris(2-pyridylmethyl)amine (TPA) and the $S = 2$ iron(IV)-oxo-halo intermediates of tris(quinolyl-2-methyl)amine (TQA) ligand have been reported to halogenate the C–H bond of cyclohexane.²³ Aliphatic C–H bond halogenations by most of the reported complexes were performed with oxidants such as PhIO or peroxides. Recently, we reported a nonheme iron(II)-benzilate complex, which, in combination with a protic acid and chloride ion, performed O_2 -dependent halogenation of aliphatic substrates with weak C–H bonds.²⁰ However, there is no report of a nonheme iron(II)- α -keto acid complex exhibiting C–H bond halogenation with O_2 . In our efforts to mimic the function of the α -KG-dependent nonheme halogenases, we

have investigated the reactivity of iron(II)- α -ketoacid-halide complexes supported by tridentate nitrogen donor ligands. We report herein the isolation, dioxygen reactivity, and ability for aliphatic C–H bond halogenation of a mononuclear iron(II)-benzoylformate-chloro complex $[(\text{phdpa})\text{Fe}(\text{BF})\text{Cl}]$ (1) and a dinuclear iron(II)-benzoylformate-chloro complex $[(1,4\text{-tpbd})\text{Fe}_2(\text{BF})_2\text{Cl}_2]$ (2) (BF = benzoylformate, phdpa = *N,N*-bis(2-pyridylmethyl)aniline, and 1,4-tpbd = *N,N,N',N'*-tetrakis-(2-pyridylmethyl)benzene-1,4-diamine).²⁴ Both the complexes activate O_2 and perform C–H bond halogenation in addition to C–H bond oxygenation. Unlike complex 1, which can halogenate the weak C–H bonds, complex 2 is able to carry out the halogenation of strong C–H bonds including that of cyclohexane. The effect of the second metal center in complex 2 on the dioxygen-dependent C–H bond halogenation is presented in this work.

RESULTS AND DISCUSSION

The iron(II)-BF-Cl complexes (**1** and **2**) were isolated from the reactions between the respective ligand, FeCl₂ and sodium benzoylformate (NaBF) in a solvent mixture (5:1) of CH₂Cl₂ and CH₃OH (Scheme 2 and Experimental Section). The UV-vis spectrum of **1** in CH₃CN exhibited broad adsorption bands at 580 nm (240 M⁻¹ cm⁻¹) and 645 nm (240 M⁻¹ cm⁻¹) (Figure S1). Similarly, complex **2** displayed adsorption bands at 592 nm (700 M⁻¹ cm⁻¹) and 650 nm (710 M⁻¹ cm⁻¹) (Figure S1). These absorption features are characteristics of BF coordinated to an iron(II) center in a bidentate mode. The absorption bands originate from the charge transfer transitions from iron(II) to π^* of the keto group of BF.^{25,26} The ¹H NMR spectra of both of the complexes in CDCl₃ exhibited paramagnetically shifted proton resonances typical of high-spin iron(II) complexes (Figures S2 and S3). Complex **2**, however, exhibited a smaller number of proton resonances compared to complex **1** in the region between 5 and 20 ppm indicating a centrosymmetric structure in solution.

The binding modes of the ligands and the geometry of the complexes were further established from X-ray diffraction studies. Complex **1** showed a mononuclear iron(II) center coordinated by the tridentate phdpa ligand and a monoanionic benzoylformate. The supporting ligand coordinates in the facial mode, and the BF is coordinated in a bidentate fashion via a carboxylate oxygen (O2) and the carbonyl oxygen (O1). A chloride ligand occupies the sixth coordination site of the iron center (Figure 1a). The Fe–O2 (carboxylate) bond distance of 2.044(2) Å is shorter than the Fe–O1 (keto) bond of 2.204(2) Å (Table 1). Complex **2** is a dinuclear system

Table 1. Selected Bond Parameters for **1** and **2**

bond distances (Å) /angles (deg)	complex 1	bond distances (Å) /angles (deg)	complex 2
Fe1–N1	2.144(2)	Fe1–N1	2.148(3)
Fe1–N2	2.441(2)	Fe1–N2	2.446(3)
Fe1–N3	2.147(2)	Fe1–N3	2.165(3)
Fe1–O1	2.204(2)	Fe1–O1	2.186(2)
Fe1–O2	2.044(2)	Fe1–O2	2.049(3)
Fe1–Cl1	2.3685(7)	Fe1–Cl2	2.390(1)
O2–Fe1–N1	152.17(8)	O2–Fe1–N1	150.92(11)
O2–Fe1–N3	93.10(8)	O2–Fe1–N3	100.65(11)
N1–Fe1–N3	100.54(8)	N1–Fe1–N3	93.58(11)
O2–Fe1–O1	75.36(7)	O2–Fe1–O1	76.27(9)
N1–Fe1–O1	87.85(7)	N1–Fe1–O1	85.68(10)
N3–Fe1–O1	167.20(8)	N3–Fe1–O1	170.82(10)
O2–Fe1–Cl1	107.13(7)	O2–Fe1–Cl2	104.41(8)
N1–Fe1–Cl1	95.27(6)	N1–Fe1–Cl2	98.88(9)
N3–Fe1–Cl1	96.86(6)	N3–Fe1–Cl2	96.74(9)
O1–Fe1–Cl1	91.93(5)	O1–Fe1–Cl2	92.42(7)
O2–Fe1–N2	86.50(8)	O2–Fe1–N2	84.39(10)
N1–Fe1–N2	74.50(8)	N1–Fe1–N2	75.01(11)
N3–Fe1–N2	73.49(8)	N3–Fe1–N2	74.74(10)
O1–Fe1–N2	99.85(7)	O1–Fe1–N2	96.26(9)
Cl1–Fe1–N2	163.96(5)	Cl2–Fe1–N2	168.92(7)

where each of the iron centers is coordinated by the N3 donors from bis(tridentate) ligand (Figure 1b). The remaining sites of each iron center are occupied by a bidentate BF and a chloride donor. The average Fe–N (pyridine) distance varies in the range 2.148(3)–2.446(3) Å, which matches well with the reported high-spin iron(II)-BF complexes.²⁵ As in **1**, the Fe–

O2 (carboxylate) bond in **2** is shorter than the Fe–O1 (keto) bond. The pyridine nitrogen N3 and the keto oxygen (O1) occupy the axial positions with the N3–Fe1–O1 angle of 170.82(10)°. The chloride ligand binds trans to the amine nitrogen (N2), and compared to Fe–N(pyridine), the Fe–N2 bond distance is much longer in both the complexes (Table 1). The two iron centers in **2** are separated at a distance of 8.739 Å and do not interact with each other as is evident from the solid state structure. The Fe–Cl bond distance of 2.390(1) Å in **2** is slightly elongated compared to that in **1** (2.3685(7) Å). Of note, the Fe–Cl distance of 2.44 Å has been reported for the structure of SyrB2 (at 1.6 Å resolution) coordinated by a chloride and α -ketoglutarate.⁴

The iron(II)-BF complexes are stable in the solid state and in solution under inert atmosphere but are sensitive to air. For an acetonitrile solution of complex **1** upon exposure to dry O₂ gas, the charge transfer bands decayed over a period of 6 h (Figure S4). For complex **2**, however, the charge transfer bands took 4 h for complete decay (Figure 2). Time-dependent ¹H

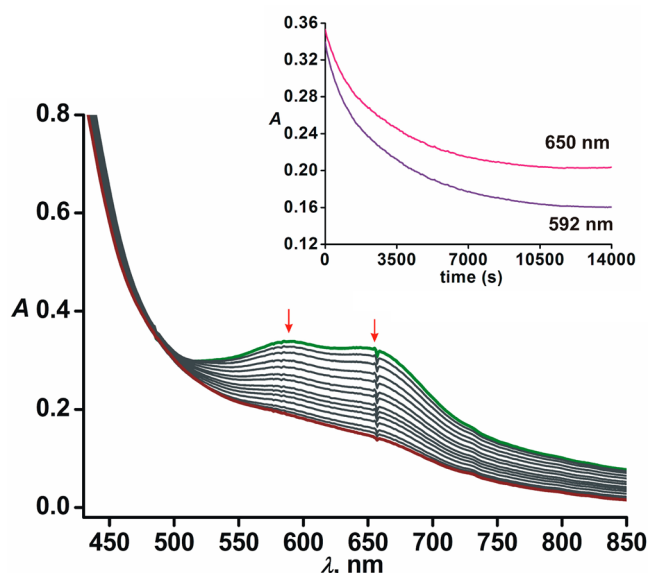


Figure 2. Time-dependent optical spectra of the reaction between **2** (0.5 mM) and dioxygen in acetonitrile at 298 K. Inset: Change in absorbance with time.

NMR spectra revealed that the coordinated BF took 50 and 8 h for complete decarboxylation to benzoate for **1** and **2**, respectively (Figure S5 and Figure 3). Although the dinuclear complex exhibited an enhanced rate of decarboxylation, there was a mismatch between the time for decay of the CT chromophore and the time taken for complete decarboxylation. Time-dependent X-band EPR studies during the reaction between **2** and dioxygen indicated that the reaction solution remained X-band EPR silent until 3 h, during which time more than 60% conversion of benzoylformate to benzoate took place (Figure S6). These observations do not support the involvement of any iron(III) species generated via one-electron oxidation of the iron(II) center without involving benzoylformate.

Upon confirmation of the conversion of BF to benzoic acid, the fate of the oxygen atoms of dioxygen was determined by 18-O labeling experiments. The GC–MS of benzoic acid showed an ion peak at m/z 122, which shifted two mass units higher to m/z 124 when the decarboxylation reaction was

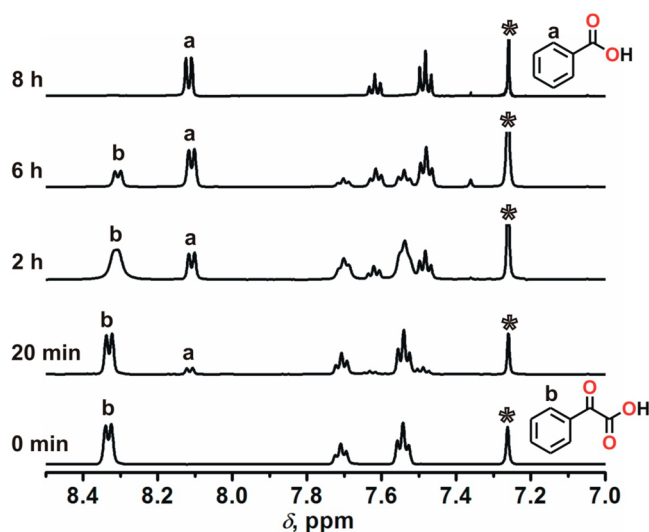


Figure 3. Time-dependent ^1H NMR (500 MHz in CDCl_3 at 298 K) spectra of benzoic acid formed in the reaction of **2** with dioxygen. The peak marked with asterisk (*) comes from residual solvent.

carried out with $^{18}\text{O}_2$ (Figure 4). These results confirmed the incorporation of one oxygen atom from dioxygen.

Enzymatic studies have established the formation of high-valent iron-oxo oxidants in the decarboxylation of α -KG.^{3,8,27} Unfortunately, no iron–oxygen intermediate was detected in the reactions of the complexes (**1** and **2**) with dioxygen. As reported with other iron(II)-BF model complexes,^{28–30} various external substrates were used to intercept in situ generated iron–oxygen oxidants. The reaction of **1** with thioanisole (20 equiv) afforded thioanisole oxide in 5% yield (Figure S7). Complex **2**, under similar experimental conditions, showed 11% conversion of thioanisole (Table 2). The labeling experiment with $^{18}\text{O}_2$ revealed around 93% incorporation of labeled oxygen into thioanisole oxide (Figure 5). However, a mixed labeling experiment with $^{16}\text{O}_2/\text{H}_2^{18}\text{O}$ did not show incorporation of labeled oxygen from water into the product, confirming that the active oxidant from **2** could not exchange its oxygen atom with water. 9,10-Dihydroanthracene, fluorene, and benzyl alcohol were oxidized to anthracene, fluorenone, and benzaldehyde, respectively, by both **1** and **2** (Table 2). An approximately 2- to 3-fold increase in the yields of oxidized

Table 2. Oxidation of Substrates with O_2 by **1** and **2**

substrate (equiv)	product(s)	mononuclear complex (1) yield (%)	dinuclear complex (2) yield (%) ^a
thioanisole (20)	thioanisole oxide	5 ± 1	11 ± 1
9,10-dihydroanthracene (10)	anthracene	25 ± 1	56 ± 2
fluorene (10)	fluorenone	10 ± 1	25 ± 1
benzyl alcohol (20)	benzaldehyde	14 ± 1	35 ± 1
cyclooctene (100)	cyclooctene oxide		24 ± 1
1-octene (100)	1,2-epoxyoctane		8 ± 0.5
<i>trans</i> -2-heptene (100)	<i>trans</i> -2-heptene oxide		29 ± 1
<i>cis</i> -2-heptene (100)	<i>cis</i> -2-heptene oxide		14 ± 1
	<i>trans</i> -2-heptene oxide		17 ± 1

^aYields were calculated on the basis of molar concentration of the complex (0.02 mmol).

products was obtained for all the substrates in the oxidation by the dinuclear complex.

Mononuclear complex **1** was unable to oxidize alkenes such as cyclooctene, 1-octene, *trans*-2-heptene, and *cis*-2-heptene. In contrast, complex **2** oxidized alkenes selectively to the corresponding epoxides but in low yields (Table 2). The reaction of **2** with cyclooctene afforded cyclooctene oxide in 24% yield (Figure S8). With *trans*-2-heptene as a substrate, only *trans*-2-heptene oxide (29%) was detected (Figure S9). However, the oxidation of *cis*-2-heptene yielded a mixture of *cis*-2-heptene oxide (14%) and *trans*-2-heptene oxide (17%) (Figures S10 and S11). 1-Octene was converted to 1,2-epoxyoctane (8%) in the reaction of **2** with dioxygen (Figure S12).

Importantly, when cyclohexene was used as a substrate in the reaction between **1** and O_2 , 3-chlorocyclohexene (4%) (Scheme 3) was formed along with 2-cyclohexenol (6%) and 2-cyclohexenone (11%) (Table 3). Similarly, for 1,4-cyclohexadiene the corresponding unsaturated chlorinated product was obtained in 5% yield (Table 3). Importantly, the dinuclear

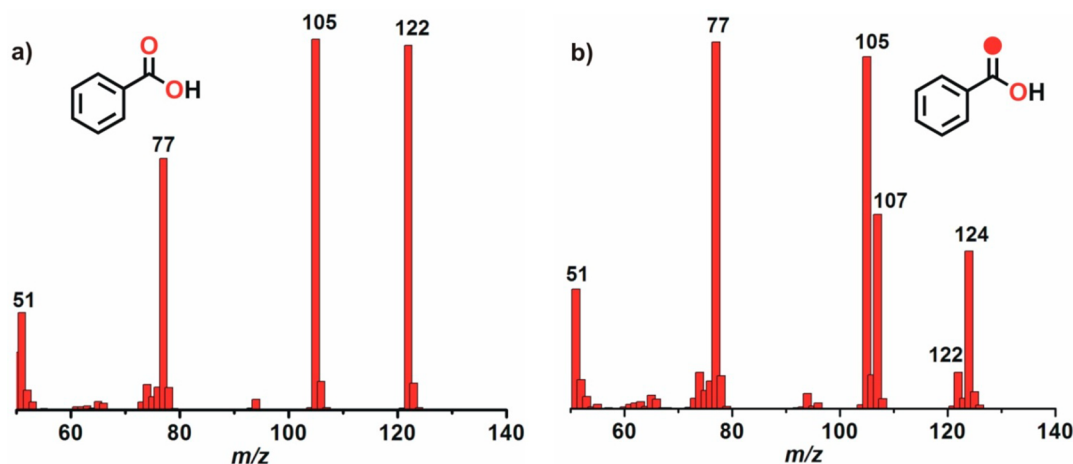


Figure 4. GC–MS of benzoic acid formed in the reaction of **2** with (a) $^{16}\text{O}_2$ and (b) $^{18}\text{O}_2$.

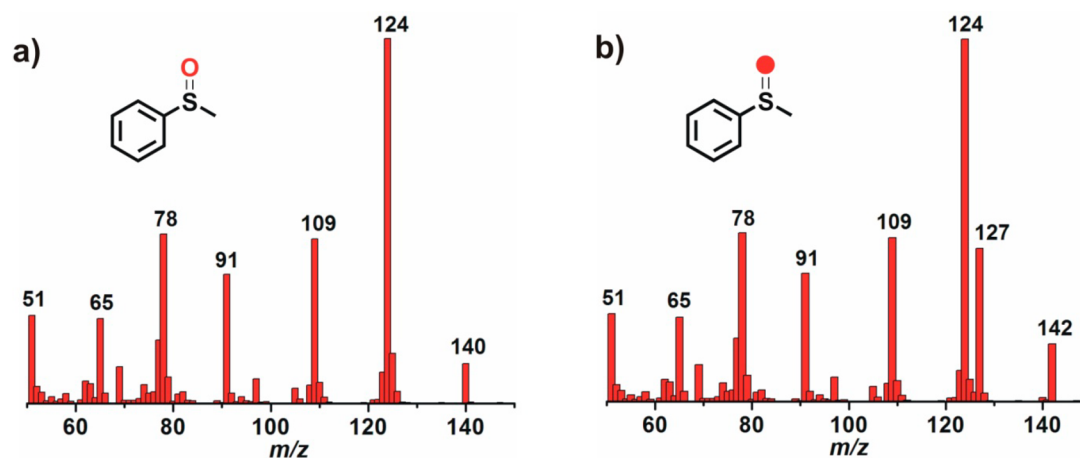
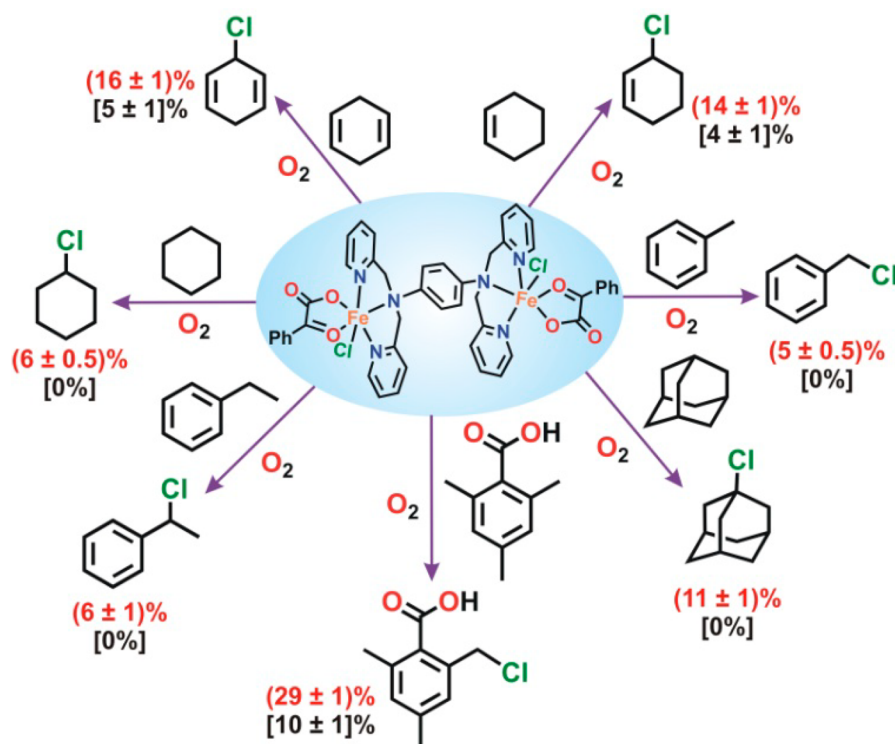


Figure 5. GC–MS of thioanisole oxide obtained from the reaction between **2** and thioanisole (20 equiv) with (a) $^{16}\text{O}_2$ and (b) $^{18}\text{O}_2$.

Scheme 3. Aliphatic C–H Bond Halogenation with O_2 by Dinuclear Complex **2** (Red)^a




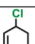
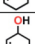
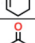

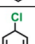
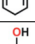

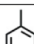
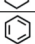
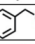
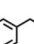
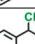


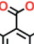
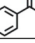

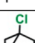


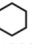
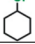

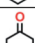
^aValues in third brackets (black) indicate the yield of chlorinated products obtained with mononuclear complex **1**.

complex **2** showed enhanced reactivity toward oxygenation as well as halogenation of alkanes. In the reaction with **2**, cyclohexene afforded 3-chlorocyclohexene in 14% yield, and the oxygenated products, 2-cyclohexanol and 2-cyclohexanone, were formed in 16% and 12%, respectively (Table 3 and Figure S13). 1,4-Cyclohexadiene was transformed to the corresponding unsaturated chlorinated product in 16% yield (Scheme 3 and Figure S14). Of note, the control experiment with a combination of FeCl_2 , sodium benzoylformate, and substrate in O_2 -saturated acetonitrile did not afford any halogenated product (Experimental Section).

The reactivity of the dinuclear complex (**2**), when compared with the mononuclear complex (**1**), increased appreciably in terms of C–H bond halogenation (Scheme 3 and Table 3). Though toluene afforded a trace amount of benzaldehyde

without any halogenated product, the active oxidant generated from **1** was not reactive enough to cleave the C–H bonds of ethylbenzene and adamantane. On the contrary, the C–H bonds of these substrates were halogenated by the dinuclear complex **2** and O_2 . Benzyl chloride and 1-phenylethyl chloride were obtained in 5–6% yield from toluene and ethylbenzene, respectively (Figures S15 and S16). Adamantane got oxidatively chlorinated to 1-chloroadamantane (11%). In the reaction, 1-adamantanol (12%) along with a negligible amount of 2-adamantanol was also formed (Figure S17). A substrate with very strong C–H bonds such as cyclohexane (100 equiv) afforded cyclohexanol (5%) and cyclohexanone (7%) without any halogenated product in the reaction with **2**. However, when the amount of cyclohexane was increased up to 1000 equiv, the formation of chlorocyclohexane (6%) (Scheme 3)

Table 3. Halogenation/Oxygenation of Aliphatic C–H Bonds with O₂ by the Iron(II)-BF Complexes

Substrate (Equiv)	Product(s)	Mononuclear complex (1) Yield (%)	Dinuclear complex (2) Yield (%) ^a
 (100)		4 ± 1	14 ± 1
		6 ± 1	16 ± 1
		11 ± 1	12 ± 1
 (100)		5 ± 1	16 ± 1
		6 ± 1	17 ± 0.5
		14 ± 1	21 ± 1
 (100)		-	5 ± 0.5
		3 ± 1	17 ± 1
 (100)		-	6 ± 1
		-	10 ± 1
		-	11 ± 1
 (10)		10 ± 1	29 ± 1
 (10)		-	11 ± 1
		-	12 ± 1
		-	<1
 (1000)		-	6 ± 0.5
		-	10 ± 1
		-	18 ± 1

^aYields were calculated on the basis of molar concentration of the complex (0.02 mmol).

was observed along with cyclohexanol (10%) and cyclohexanone (18%) (Figure S18). 2,4,6-Trimethylbenzoic acid (TMBA) was used as a substrate to evaluate the effect of the carboxylate group on C–H bond halogenation. TMBA underwent benzylic C–H bond halogenation by 1 and 2 affording 10% and 29% halogenation product, respectively (Table 3 and Figure S19). The higher yield of the chlorinated product from TMBA compared to those from toluene and ethylbenzene suggested the role of the –COOH group of TMBA in directing the reaction toward the halogenation pathway. Thus, dinuclear complex 2 ensured not only the halogenation of strong C–H bonds including those of

cyclohexane, but also an approximately 2–3 fold increase in the yields of halogenated products was observed for substrates with weak C–H bonds. Although the iron centers in the dinuclear complex are separated at a distance of 8.739 Å, the two are connected through a benzene-14-diamine spacer. It is therefore hypothesized that the electronic effect of one site influences the reactivity of the other in terms of C–H bond halogenation/hydroxylation. However, the exact reason for increased reactivity in the dinuclear complex remains unclear.

The difference in the amount of halogenated products from substrates of varying C–H bond strengths along with the results of control experiments (Experimental Section) indicated the involvement of a metal-based oxidant in the halogenation reactions. The yield of the halogenated product of cyclohexane did not increase upon addition of Bu₄NCl in the reaction with 2 and dioxygen. From the relative percentage of oxygenated products in competitive oxidation of toluene and toluene-*d*₈ by 2, a KIE value of 9.3 was estimated (Figure S20). While the halogenation reactions of aliphatic substrates were not affected by the presence of radical scavengers such as *tert*-butanol and 1,4-benzoquinone, the addition of thioanisole inhibited the halogenation of cyclohexane completely. Furthermore, complex 2 selectively oxidized cyclobutanol to cyclobutanone (Figure S21). These results suggested in situ generation of a two-electron oxidant and ruled out the involvement of any free-radical mechanism in the reaction pathway.

Therefore, a metal-based oxidant is proposed to perform the halogenation of C–H bonds. By analogy to other reported iron(II)- α -keto acid complexes, a putative iron(IV)-oxo species is generated in situ upon reductive activation of O₂ at the iron(II) center and subsequent decarboxylation of the coordinated α -keto acid (Scheme S1).^{28,30} Since the iron centers in both the complexes (1 and 2) are coordinatively saturated, one of the labile donors (pyridine or keto oxygen of BF) may dissociate to activate dioxygen at a five-coordinate iron(II) center leading to the generation of the iron-oxo oxidant. The relatively strong binding of chloride anion possibly blocks the labile coordination site at the iron center preventing exchange between water and the oxygen atom of the active oxidant.¹⁵ The iron-oxo species abstracts the hydrogen atom from a C–H bond of substrate. The resulting iron(III)-hydroxo-chloro species in the solvent cage would then react with the alkyl radical to yield hydroxylated (via OH[•] rebound) or halogenated (via Cl[•] rebound) products. Here the reaction pathway differs from the enzymatic mechanism because the preferred Cl[•] rebound step directs the selectivity in halogenases. The low yields of halogenated product with 1 and 2 suggested that the Cl[•] rebound was slower compared to the cage escape of the alkyl radical and subsequent reaction with O₂.³¹ A high 3°/2° value for adamantane oxidation indicated a longer lifetime of the resulting alkyl radical. This was further supported by the results of the oxidation of

Table 4. Yields of Different Products from the Reaction of Complex 2 and Cyclohexane (1000 equiv) in the Presence of Varying Amounts of CCl₃Br^a

CCl ₃ Br (equiv)	chlorocyclohexane (%)	cyclohexanol (%)	cyclohexanone (%)	bromocyclohexane (%)
0	6	10	18	0
2	6	8	11	11
5	6	8	9	12

^aYields were calculated on the basis of molar concentration of the complex (0.02 mmol).

cyclohexane by **2** in the presence of varying amounts of alkyl radical trap CCl_3Br (1–5 equiv) (Table 4). With 5 equiv of CCl_3Br , the yield of chlorocyclohexane remained the same (6%), whereas the yields of cyclohexanol and cyclohexanone decreased to 8–9% along with 12% bromocyclohexane. The cage escape alkyl radical reacted with O_2 and with CCl_3Br resulting in oxygenated or brominated products, respectively. That observation supported a low alcohol-to-ketone ratio in the oxidation of cyclohexane. In the absence of any substrate, the putative iron-oxo oxidant decayed to some unidentified iron(III) product as observed in the X-band EPR spectrum (Figure S6).

CONCLUSIONS

We have developed two nonheme iron(II)- α -keto acid complexes that activated the C–H bonds of aliphatic substrates with O_2 to form the corresponding halogenated product. The dinuclear complex exhibited enhanced reactivity compared to the mononuclear complex. Unlike enzyme systems, the formation of hydroxylated/oxidized products could not be avoided and the halogenated products were detected in low yields. Yet the complexes presented here represent the only examples of nonheme iron(II)- α -keto acid complexes exhibiting bioinspired C–H bond halogenation. The strong iron-chloro bond and slow rebound of chloride radical to substrate-derived alkyl radical resulted in low yield and selectivity in halogenation reactions. Design of supporting ligands incorporating electronic/structural features for enhancing the rate of chloride rebound step and deactivating the hydroxide rebound step might allow achievement of selective halogenation of aliphatic C–H bonds with nonheme iron complexes and dioxygen.

EXPERIMENTAL SECTION

Materials and Methods. All chemicals and reagents were purchased from commercial sources and were used without further purification unless otherwise mentioned. Solvents were distilled and dried before use. Preparation and handling of air-sensitive materials were carried out under inert atmosphere in a glovebox. The ligands, *N,N*-bis(2-pyridylmethyl)aniline (phdpa) and *N,N,N',N'*-tetrakis(2-pyridylmethyl)benzene-1,4-diamine (1,4-tpbd), were prepared following reported procedures.²⁴

Fourier transform infrared spectroscopy on KBr pellets was performed on a Shimadzu FT-IR 8400S instrument. Elemental analyses were performed on a PerkinElmer 2400 series II CHN analyzer. Electrospray ionization (ESI) mass spectra were recorded with a Waters QTOF Micro YA263 instrument. Solution electronic spectra (single and time-dependent) were measured on an Agilent 8453 diode array spectrophotometer. All room temperature NMR spectra were collected on a Bruker Avance 500 MHz spectrometer. X-band EPR spectra were recorded on a JEOL JES-FA 200 instrument with 100 kHz magnetic modulation, a microwave power of 2.00 mW, and a microwave frequency of 9.1195 GHz. GC–MS measurements were carried out with a PerkinElmer Clarus 600 using an Elite 5 MS (30 m \times 0.25 mm \times 0.25 μm) column with a maximum temperature of 300 °C. Labeling experiments were carried out with $^{18}\text{O}_2$ gas (99 atom %) or H_2^{18}O (98 atom %) purchased from Icon Services Inc.

Synthesis of Metal Complexes. $[(\text{phdpa})\text{Fe}^{\text{II}}(\text{BF})(\text{Cl})]$ (**1**). Anhydrous FeCl_2 (0.127 g, 1.0 mmol) was added to a solution of phdpa ligand (0.275 g, 1.0 mmol) in 5 mL of dichloromethane, and the mixture was vigorously stirred for 12 h in a glovebox. To the mixture was added a methanolic solution (1 mL) of sodium benzoylformate (0.172 g, 1.0 mmol) dropwise. The resulting green solution was allowed to stir for 12 h and then dried. The residue obtained was dissolved in dichloromethane (10 mL) and filtered. The filtrate was then concentrated, and the resulting green solid was

collected by filtration. X-ray quality single-crystals were obtained by slow evaporation of solvent from a solution of the complex in dichloromethane and hexane mixture. Yield: 0.386 g (75%). Anal. Calcd for $\text{C}_{26}\text{H}_{22}\text{ClFeN}_3\text{O}_3$ (515.77 g/mol): C, 60.55; H, 4.30; N, 8.15. Found: C, 60.43; H, 4.09; N, 8.17%. IR (cm^{-1}): 3433(br), 3068(w), 2924(w), 2854(w), 1664(vs), 1630(m), 1601(s), 1493(w), 1443(m), 1236(m), 762(m), 692(m). UV–vis in CH_3CN λ_{max} , nm (ϵ , $\text{M}^{-1}\text{cm}^{-1}$): 386 (1315), 580 (240), 645 (240). ^1H NMR (500 MHz, CDCl_3): δ 52.0, 47.1, 29.4, 24.7, 17.2, 14.4, 11.8, 9.2, 7.9, 5.7, 5.5, 3.9, 3.2, 2.9, 2.0, –0.7, –13.6 ppm.

$[(1,4\text{-tpbd})\text{Fe}_2^{\text{II}}(\text{BF})_2\text{Cl}_2]$ (**2**). Anhydrous FeCl_2 (0.254 g, 2.0 mmol) was added to a solution of 1,4-tpbd ligand (0.473 g, 1.0 mmol) in 5 mL of dichloromethane. The mixture was vigorously stirred for 12 h in a glovebox. A methanolic solution (1 mL) of sodium benzoylformate (0.344 g, 2.0 mmol) was then added dropwise to the reaction mixture. The resulting green solution was allowed to stir for 12 h and then dried. The residue obtained was dissolved in dichloromethane (10 mL) and filtered. The filtrate was then concentrated, and the green solid was collected by filtration. X-ray quality single-crystals were obtained by slow evaporation of solvent from the solution of the complex in a mixture of dichloromethane and hexane. Yield: 0.638 g (67%). Anal. Calcd for $\text{C}_{46}\text{H}_{38}\text{Cl}_2\text{Fe}_2\text{N}_6\text{O}_6$ (953.43 g/mol): C, 57.95; H, 4.02; N, 8.81. Found: C, 57.31; H, 3.85; N, 8.70%. IR (cm^{-1}): 3433(br), 3063(w), 2924(w), 1661(s), 1628(m), 1603(m), 1514(w), 1479(w), 1438(w), 1315(w), 1238(s), 774(m), 690(w). UV–vis in CH_3CN λ_{max} , nm (ϵ , $\text{M}^{-1}\text{cm}^{-1}$): 390 (2490), 592 (700), 650 (710). ^1H NMR (500 MHz, CDCl_3): δ 52.9, 49.0, 36.1, 24.3, 17.3, 9.9, 9.3, 6.5, 5.7, 5.4, 4.1, 3.9, 3.8, 3.7, 3.1, 2.8, 1.9, –7.9 ppm.

Reactivity with Dioxygen. A solution of the complex (**1** or **2**) (0.02 mmol) in 10 mL of dioxygen-saturated CH_3CN was allowed to stir at room temperature. After the reaction, the solvent was removed under reduced pressure, and the residue was treated with 10 mL of 3 M HCl. The organic products were extracted with diethyl ether (3 \times 20 mL), and the organic phases were washed with brine solution. The combined organic part was dried over Na_2SO_4 and filtered. The solvent was then evaporated to dryness. The organic products were analyzed by ^1H NMR spectroscopy or by GC–MS.

Reactions of Iron(II) Complexes with Thioanisole. Each of the iron(II)-BF-Cl complexes (0.02 mmol) was dissolved in 10 mL of dry acetonitrile. To the resulting solution was added thioanisole (20 equiv). Pure dry dioxygen was purged through the solution for 5 min and was allowed to stir at room temperature under oxygen atmosphere. The color of the solution slowly changed from green to yellowish-green. After the reaction, the solution was concentrated under reduced pressure and treated with 10 mL of 3 M HCl. The organic products were extracted with diethyl ether (3 \times 20 mL) and dried over anhydrous sodium sulfate. The organic layer was filtered and evaporated to dryness. The products were analyzed by ^1H NMR and GC–MS. Quantification of the oxidized organic substrates were performed by comparing the peak area associated with two *ortho*-protons of benzoic acid (δ 8.11 ppm) with the peak area for the protons of the oxidized substrate.

^1H NMR (500 MHz, CDCl_3 , 298 K) data of organic products: benzoic acid δ (ppm) 8.11 (d, 2H), 7.63 (t, 1H), 7.48 (t, 2H); benzoylformic acid δ (ppm) 8.31 (d, 2H), 7.70 (t, 1H), 7.57 (t, 2H); thioanisole oxide: δ (ppm) 7.66 (m, 2H), 7.52 (m, 3H), 2.73 (s, 3H).

Reactions of Iron(II)-BF-Cl Complexes with Alkanes. The iron(II)-BF-Cl complex (0.02 mmol) was dissolved in 2 mL of dry acetonitrile. To the resulting solution was added an excess amount of substrate. Pure dry oxygen was purged through the solution and was allowed to stir at room temperature. After the oxidation, the iron complex was decomposed by addition of 1 mL of 1 M H_2SO_4 solution. Organic products were extracted by diethyl ether, and the organic layer was dried over anhydrous sodium sulfate. The organic products were then analyzed by GC–MS. The oxidized products were quantified by comparison of their GC retention times and GC–MS with those of authentic compounds. The halogenated products were quantified by comparison of the relative peak area of the halogenated products with that of naphthalene.

Reactions of iron(II)-BF-Cl with Alkenes. The iron(II)-BF-Cl complex (0.02 mmol) was dissolved in 2 mL of dry acetonitrile. To the resulting solution was added an excess amount of substrate. Pure dry oxygen was purged through the solution and was allowed to stir at room temperature. After the oxidation, the resulting solution was then passed through a 15 cm silica column (60–120 mesh size) using dichloromethane/diethyl ether as eluent. The combined organic phase was then analyzed by GC–MS. Quantification of the oxidized products was calculated using standard calibration curves obtained using authentic compounds and naphthalene as a standard which was added to the reaction mixture after desired reaction time but prior to separation through column.

Control Experiments. Separate control experiments were performed with phdpa/1,4-tpbd ligand (0.02 mmol) and sodium benzoylformate (1 equiv) in the presence of substrate (100 equiv of cyclohexene or 1000 equiv of cyclohexane) in O₂-saturated acetonitrile. Another control experiment was performed with phdpa ligand (0.02 mmol) and iron(II) chloride (1 equiv) in the presence of substrate in O₂-saturated acetonitrile solvent. No oxidized/halogenated product derived from substrate was formed in all the cases. Additionally, the combination of FeCl₂ (0.02 mmol), sodium benzoylformate (1 equiv), and cyclohexene (100 equiv) or cyclohexane (1000 equiv) in O₂-saturated acetonitrile does not afford any halogenated product.

Competitive Oxidation Reaction. Competitive oxidation reactions are carried out by dinuclear complex **2** (0.02 mmol) with thioanisole (50 equiv) and cyclohexane (1000 equiv). In the reaction, only 9% thioanisole oxide was formed along with trace amounts of chlorocyclohexane (approx 1%), cyclohexanol (1%), and cyclohexanone (5%).

X-ray Crystallographic Data Collection and Refinement and Solution of Structures. X-ray single-crystal data for **1** and **2** were collected at 120 K (Table 5) using Mo K α (λ = 0.7107 Å) radiation on a SMART-APEX diffractometer equipped with a CCD area detector. Data collection, data reduction, and structure solution and refinement were carried out using the software package of APEX II.³² The structure was solved by direct methods and subsequent Fourier analyses and refined by the full-matrix least-squares method based on

F^2 with all observed reflections.³³ The non-hydrogen atoms were treated anisotropically. Routine SQUEEZE³⁴ was applied to intensity data of complex **2** to take into account the disordered solvent molecules. CCDC 1581677 and 1581678 contain the supplementary crystallographic data for **1** and **2**, respectively. The data can be obtained free of charge from the Cambridge Crystallographic Data Centre via www.ccdc.cam.ac.uk/data_request/cif.

■ ASSOCIATED CONTENT

§ Supporting Information

The Supporting Information is available free of charge on the ACS Publications website at DOI: 10.1021/acs.inorgchem.8b00421.

Spectral and crystallographic data (PDF)

Accession Codes

CCDC 1581677–1581678 contain the supplementary crystallographic data for this paper. These data can be obtained free of charge via www.ccdc.cam.ac.uk/data_request/cif, or by emailing data_request@ccdc.cam.ac.uk, or by contacting The Cambridge Crystallographic Data Centre, 12 Union Road, Cambridge CB2 1EZ, UK; fax: +44 1223 336033.

■ AUTHOR INFORMATION

Corresponding Author

*E-mail: ictkp@iacs.res.in.

ORCID

Tapan Kanti Paine: 0000-0002-4234-1909

Notes

The authors declare no competing financial interest.

■ ACKNOWLEDGMENTS

T.K.P. gratefully acknowledges the Science and Engineering Research Board (SERB), India for the financial support (Project: EMR/2014/000972). R.D.J. thanks CSIR for a research fellowship.

■ REFERENCES

- (1) Bollinger, J. M., Jr.; Chang, W.-C.; Matthews, M. L.; Martinie, R. J.; Boal, A. K.; Krebs, C. 2-Oxoglutarate-Dependent Oxygenases; Royal Society of Chemistry: Cambridge, U.K., 2015; pp 95–122.
- (2) Galonić, D. P.; Barr, E. W.; Walsh, C. T.; Bollinger, J. M., Jr.; Krebs, C. Two interconverting Fe(IV) intermediates in aliphatic chlorination by the halogenase CytC3. *Nat. Chem. Biol.* **2007**, *3*, 113–116.
- (3) Matthews, M. L.; Krest, C. M.; Barr, E. W.; Vaillancourt, F. H.; Walsh, C. T.; Green, M. T.; Krebs, C.; Bollinger, J. M., Jr. Substrate-Triggered Formation and Remarkable Stability of the C–H Bond-Cleaving Chloroferryl Intermediate in the Aliphatic Halogenase, SyrB2. *Biochemistry* **2009**, *48*, 4331–4343.
- (4) Blasiak, L. C.; Vaillancourt, F. H.; Walsh, C. T.; Drennan, C. L. Crystal structure of the non-haem iron halogenase SyrB2 in syringomycin biosynthesis. *Nature* **2006**, *440*, 368–371.
- (5) Khare, D.; Wang, B.; Gu, L.; Razelun, J.; Sherman, D. H.; Gerwick, W. H.; Håkansson, K.; Smith, J. L. Conformational switch triggered by α -ketoglutarate in a halogenase of curacin A biosynthesis. *Proc. Natl. Acad. Sci. U. S. A.* **2010**, *107*, 14099–14104.
- (6) Wong, C.; Fujimori, D. G.; Walsh, C. T.; Drennan, C. L. Structural Analysis of an Open Active Site Conformation of Nonheme Iron Halogenase CytC3. *J. Am. Chem. Soc.* **2009**, *131*, 4872–4879.
- (7) Galonić, D.; Fujimori, D.; Barr, E. W.; Matthews, M. L.; Koch, G. M.; Yonce, J. R.; Walsh, C. T.; Bollinger, J. M., Jr.; Krebs, C.; Riggs-Gelasco, P. J. Spectroscopic Evidence for a High-Spin Br-Fe(IV)-Oxo Intermediate in the α -Ketoglutarate-Dependent Halogenase CytC3 from *Streptomyces*. *J. Am. Chem. Soc.* **2007**, *129*, 13408–13409.

Table 5. Crystallographic Data for Complexes **1** and **2**

param	1	2
empirical formula	C ₂₆ H ₂₂ ClFeN ₃ O ₃	C ₄₆ H ₃₈ Cl ₂ Fe ₂ N ₆ O ₆
fw	515.76	953.42
cryst syst	monoclinic	triclinic
space group	Cc	P $\bar{1}$
a, Å	19.6859(19)	9.278(2)
b, Å	8.4165(9)	9.783(3)
c, Å	16.0097(16)	12.934(3)
α , deg	90	88.827(7)
β , deg	118.015(2)	88.073(7)
γ , deg	90	82.412(7)
V, Å ³	2341.8(4)	1163.0(5)
Z	4	1
D _{calc} g/cm ³	1.463	1.361
μ Mo K α , mm ^{−1}	0.792	0.791
F(000)	1064.0	490.0
θ range, deg	2.344–28.911	1.575–26.783
reflns collected	15 082	14 907
reflns unique	5100	4734
R(int)	0.0274	0.0767
data [$I > 2\sigma(I)$]	4874	3227
params refined	307	280
GOF on F^2	0.715	0.977
R1 [$I > 2\sigma(I)$]	0.0256	0.0550
wR2	0.0867	0.1527

- (8) Wong, S. D.; Srncic, M.; Matthews, M. L.; Liu, L. V.; Kwak, Y.; Park, K.; Bell, C. B., III; Alp, E. E.; Zhao, J.; Yoda, Y.; Kitao, S.; Seto, M.; Krebs, C.; Bollinger, J. M., Jr.; Solomon, E. I. Elucidation of the Fe(IV)=O intermediate in the catalytic cycle of the halogenase SyrB2. *Nature* **2013**, *499*, 320–323.
- (9) Matthews, M. L.; Neumann, C. S.; Miles, L. A.; Grove, T. L.; Booker, S. J.; Krebs, C.; Walsh, C. T.; Bollinger, J. M., Jr. Substrate positioning controls the partition between halogenation and hydroxylation in the aliphatic halogenase, SyrB2. *Proc. Natl. Acad. Sci. U. S. A.* **2009**, *106*, 17723–17728.
- (10) Kulik, H. J.; Drennan, C. L. Substrate Placement Influences Reactivity in Non-heme Fe(II) Halogenases and Hydroxylases. *J. Biol. Chem.* **2013**, *288*, 11233–11241.
- (11) Martinie, R. J.; Livada, J.; Chang, W.-c.; Green, M. T.; Krebs, C.; Bollinger, J. M., Jr.; Silakov, A. Experimental Correlation of Substrate Position with Reaction Outcome in the Aliphatic Halogenase, SyrB2. *J. Am. Chem. Soc.* **2015**, *137*, 6912–6919.
- (12) Pandian, S.; Vincent, M. A.; Hillier, I. H.; Burton, N. A. Why does the enzyme SyrB2 chlorinate, but does not hydroxylate, saturated hydrocarbons? A density functional theory (DFT) study. *Dalton Trans.* **2009**, 6201–6207.
- (13) de Visser, S. P.; Latifi, R. Carbon Dioxide: A Waste Product in the Catalytic Cycle of α -Ketoglutarate Dependent Halogenases Prevents the Formation of Hydroxylated By-Products. *J. Phys. Chem. B* **2009**, *113*, 12–14.
- (14) Friese, S. J.; Kucera, B. E.; Young, V. G., Jr.; Que, L., Jr.; Tolman, W. B. Iron(II) Complexes of Sterically Bulky α -Ketocarboxylates. Structural Models for α -Ketoacid-Dependent Non-heme Iron Halogenases. *Inorg. Chem.* **2008**, *47*, 1324–1331.
- (15) Planas, O.; Clémancey, M.; Latour, J.-M.; Company, A.; Costas, M. Structural modeling of iron halogenases: synthesis and reactivity of halide-iron(IV)-oxo compounds. *Chem. Commun.* **2014**, *50*, 10887–10890.
- (16) Kojima, T.; Leising, R. A.; Yan, S.; Que, L., Jr. Alkane Functionalization at Nonheme Iron Centers. Stoichiometric Transfer of Metal-Bound Ligands to Alkane. *J. Am. Chem. Soc.* **1993**, *115*, 11328–11335.
- (17) Barton, D. H. R.; Hu, B.; Li, T.; MacKinnon, J. The Importance of Pyridine Complexation on Selective Oxidation within the Fe(III)-Fe(V) Manifold in Gif Chemistry. *Tetrahedron Lett.* **1996**, *37*, 8329–8332.
- (18) Comba, P.; Wunderlich, S. Iron-Catalyzed Halogenation of Alkanes: Modeling of Nonheme Halogenases by Experiment and DFT Calculations. *Chem. - Eur. J.* **2010**, *16*, 7293–7299.
- (19) Vardhaman, A. K.; Barman, P.; Kumar, S.; Sastri, C. V.; Kumar, D.; de Visser, S. P. Mechanistic insight into halide oxidation by non-heme iron complexes. Haloperoxidase versus halogenase activity. *Chem. Commun.* **2013**, *49*, 10926–10928.
- (20) Chatterjee, S.; Paine, T. K. Hydroxylation versus Halogenation of Aliphatic C-H Bonds by a Dioxygen-Derived Iron–Oxygen Oxidant: Functional Mimicking of Iron Halogenases. *Angew. Chem., Int. Ed.* **2016**, *55*, 7717–7722.
- (21) Rohde, J.-U.; Stubna, A.; Bominaar, E. L.; Münck, E.; Nam, W.; Que, L., Jr. Nonheme Oxoiron(IV) Complexes of Tris(2-pyridylmethyl)amine with *cis*-Monoanionic Ligands. *Inorg. Chem.* **2006**, *45*, 6435–6445.
- (22) England, J.; Guo, Y.; Van Heuvelen, K. M.; Cranswick, M. A.; Rohde, G. T.; Bominaar, E. L.; Münck, E.; Que, L., Jr. A More Reactive Trigonal-Bipyramidal High-Spin Oxoiron(IV) Complex with a *cis*-Labile Site. *J. Am. Chem. Soc.* **2011**, *133*, 11880–11883.
- (23) Puri, M.; Biswas, A. N.; Fan, R.; Guo, Y.; Que, L., Jr. Modeling Non-Heme Iron Halogenases: High-Spin Oxoiron(IV)–Halide Complexes That Halogenate C–H Bonds. *J. Am. Chem. Soc.* **2016**, *138*, 2484–2487.
- (24) Hazell, A.; McKenzie, C. J.; Nielsen, L. P. Synthesis, structural characterisation and electronic behaviour of iron(II) and nickel(II) complexes of N,N-bis(2-pyridylmethyl)aniline. *Polyhedron* **2000**, *19*, 1333–1338.
- (25) Chiou, Y.-M.; Que, L., Jr. Models for α -Keto Acid-Dependent Non-Heme Iron Enzymes: Structures and Reactivities of $[\text{Fe}^{\text{II}}(\text{L})-(\text{O}_2\text{CCOPh})](\text{ClO}_4)$ Complexes. *J. Am. Chem. Soc.* **1995**, *117*, 3999–4013.
- (26) Pavel, E. G.; Zhou, J.; Busby, R. W.; Gunsior, M.; Townsend, C. A.; Solomon, E. I. Circular Dichroism and Magnetic Circular Dichroism Spectroscopic Studies of the Non-Heme Ferrous Active Site in Clavamine Synthase and Its Interaction with α -Ketoglutarate Cosubstrate. *J. Am. Chem. Soc.* **1998**, *120*, 743–753.
- (27) Krebs, C.; Galonić Fujimori, D.; Walsh, C. T.; Bollinger, J. M., Jr. Non-Heme Fe(IV)–Oxo Intermediates. *Acc. Chem. Res.* **2007**, *40*, 484–492.
- (28) Mukherjee, A.; Martinho, M.; Bominaar, E. L.; Münck, E.; Que, L., Jr. Shape-Selective Interception by Hydrocarbons of the O_2 -Derived Oxidant of a Biomimetic Nonheme Iron Complex. *Angew. Chem., Int. Ed.* **2009**, *48*, 1780–1783.
- (29) Sheet, D.; Halder, P.; Paine, T. K. Enhanced Reactivity of a Biomimetic Iron(II) α -Keto Acid Complex through Immobilization on Functionalized Gold Nanoparticles. *Angew. Chem., Int. Ed.* **2013**, *52*, 13314–13318.
- (30) Paine, T. K.; Que, L., Jr. Dioxygen Activation by Biomimetic Iron Complexes of α -Keto Acids and α -Hydroxy Acids. *Struct. Bonding (Berlin, Ger.)* **2014**, *160*, 39–56.
- (31) Barton, D. H. R.; Doller, D. The Selective Functionalization of Saturated Hydrocarbons: Gif Chemistry. *Acc. Chem. Res.* **1992**, *25*, 504–512.
- (32) APEX 2, v2.1-0; Bruker AXS: Madison, WI, 2006.
- (33) Sheldrick, G. M. *SHELXL-97, Program for Crystal Structure Refinement*; University of Göttingen: Göttingen, Germany, 1997.
- (34) Spek, A. L. *PLATON. A Multipurpose Crystallographic Tool*; Utrecht University: Utrecht, The Netherlands, 2002.